Available online at www.sciencedirect.com

SCIENCE DIRECT

Diamond & Related Materials 15 (2006) 324 – 328

DIAMOND AND RELATED MATERIALS

www.elsevier.com/locate/diamond

Characteristics of ultra-nano-crystalline diamond films grown on the porous anodic alumina template

Ying-Chieh Chen [a,*], Chia-Yun Chen [a], Nyan-Hwa Tai [a], Yen-Chih Lee [a], Su-Jien Lin [a], I-Nan Lin [b,*]

[a] *Department of Material Science and Engineering, National Tsing-Hua University, Hsin-Chu 300, Taiwan R. O. C.*
[b] *Department of Physics, Tamkang University, Tamsui 251, Taiwan R. O. C.*

Available online 10 October 2005

Abstract

Nanodiamond films containing uniformly small diamond grains (<20 nm) were synthesized using porous anodic alumina (PAA) as template in conjunction with bias-enhanced nucleation growth (BEG) process. PAA with uniform pore size distribution is required and the bottom of channel should be free of residual alumina layer for the purpose of effectively nucleating diamond seeds. Thus obtained PAA-patterns can then effectively enhance the formation of diamond nuclei, resulting in patterned nanodiamond films, which possess superior electron field emission properties to the non-patterned nanodiamond films. Benefit of PAA patterning process on improving the electron field emission properties of the nanodiamond films is ascribed to the suppression on the formation of trans-polyacetylene layer and the presence of hillock structure, which facilitates the electron transport from Si surface to top surface of nanodiamond.

Keywords: NCD; PAA; Electron field emission

1. Introduction

Diamond is a promising material for various types of electronic micro- or nano-fabricated electron devices [1] because of its wide-bandgap, high carrier transport speed, high breakdown field and negative electron affinity. Recently, there is a wide interest in improving the electron field emission properties of diamond films due to marvelous stable properties owned by diamond films. One of the possible routes for increasing the electron field emission capacity of diamond films is to reduce the grain size [2]. The other possible route is to increase the enhancement factor by increasing the emitter's aspect ratio [3]. However, high hardness and chemical inertness of nanodiamond make it difficult to form arbitrary shapes by post-processes. The leading nanotechnologies for sub-optical (10–200 nm) fabrication, such as X-ray lithography (XRL) [4] and electron-beam lithography (EBL) [5], have some serious drawbacks; the resolution of XRL is limited by diffraction effects to 20–50 nm, whereas the electron-beam lithography (EBL) is characterized by low sample throughput and high cost.

Porous anodic alumina (PAA) have received significant attention for patterning process, due to its inherent nature of low cost, large-area, controllable pore size and reliable fabrication [6]. PAA with pore diameters ranging from nano-meters to submicro-meters have thus been used extensively as templates for the fabrications of nanowires with different composition and structure [7,8]. Compared to other materials for nano-sphere lithography, such as polystyrene membranes [9] PAA membranes possess a much higher pore density, up to about 10^{11}pores/cm^2 [10]. Moreover diameter and density of pores can be controlled by varying the anodization voltage and electrolyte types [11].

In this paper, we have developed a nano-fabrication method, combining PAA and bias enhanced growth (BEG) technique, for the synthesis of nanodiamond films. The benefit of such a nano-fabrication process on the electron field emission properties of obtained materials is demonstrated.

2. Experimental

In this study, nanodiamond films were grown on n-type (100) Si substrate, which was patterned by porous anodic

* Corresponding author. I-Nan Lin is to be contacted at 151 Yin-Chuan Rd., Tamsui, Taipei, Taiwan 251, R. O. C.
E-mail addresses: elvis.bobo@msa.hinet.net (Y.-C. Chen), inanlin@mail.tku.edu.tw (I.-N. Lin).

0925-9635/$ - see front matter © 2005 Elsevier B.V. All rights reserved.
doi:10.1016/j.diamond.2005.08.062

alumina (PAA). A two-step process was adopted to improve the uniformity of the PAA layer. Aluminum films were first deposited on Si substrate by electron beam evaporation process (ULVAC). The first anodization process was carried out in 10% phosphoric acid solution (H_3PO_4) at 10 °C and 100 V for several minutes. In order to improve uniformity of pores, the first PAA layer formed in stage I was removed using mixture solution of 4 vol% CrO_3 and 10 vol% H_3PO_4 acid. The remaining aluminum was re-anodized under the same conditions until the total film was fully oxidized (stage II). The second anodization was proceeded with the same condition as the first step to improve the uniformity of the ordered honeycomb array. After second anodization, the PAA films were dipped in 5% phosphoric acid at 40 °C for 60 min for removing barrier layer and for adjusting pore size.

The nanodiamond films were then grown on the PAA honeycomb pattern by bias enhanced growth (BEG) techniques in a 2.45 GHz ASTeX MPECVD system. The deposition process was carried out under methane and hydrogen plasma (CH_4/H_2=45/300 sccm, 55 Torr), with continuous negative DC bias voltage to substrate (−125 V), using at 1500 W microwave power, for 5–20 min. Morphologies of PAA and diamond films were characterized by field emission scanning electron microscopy (FESEM, JEOL 6010), atomic force microscopy (AFM, PARK), and Raman spectroscopy (Renishaw). Electron field emission from diamond films were measured by a parallel-plate setup, in which the cathode-to-anode distance is controlled by a micrometer attached to a rod about 3 mm in diameter. The current–voltage properties were measured by an electron source unit (Keithley, Model 237). The important parameters such as turn-on field (E_0), field enhancement factor (β) and effective work function (Ψ) were exact from the current–voltage curves using Fowler–Nordheim theory [14].

3. Results and discussion

In general, the anodization of aluminum layer proceeds in 4 stages [6]: (I) formation of nanopores, which spread over the Al-layer gradually and finally covered the entire substrates. In this step, the anodizing current (J) monotonously decreases with time (region I, Fig. 1(a)); (II) propagation of pores downward to form channels, resulting in monotonically decrease in anodizing current with abrupt change in the slope of anodizing current–time (J–t) curve (region II, Fig. 1(a)). The anodizing current reaches the minimum value at the end of stage II, indicating that all the aluminum layer is oxidized and (III) the dissolution of alumina starts, which results in the increase in anodization current (region III, Fig. 1(a)); and (IV) transition of aluminum anodization process to silicon oxidation process, causing the 2nd reversion of anodizing current (region IV, Fig. 1(a)). It should be noted that in order to improve the uniformity of the anodized pores, the first porous anodic alumina (PAA) layer resulted at the end of stage I was usually removed by chemical etching process. The above-described PAA process was carried out in 10% phosphoric acid and the process is designated as two-step PAA process.

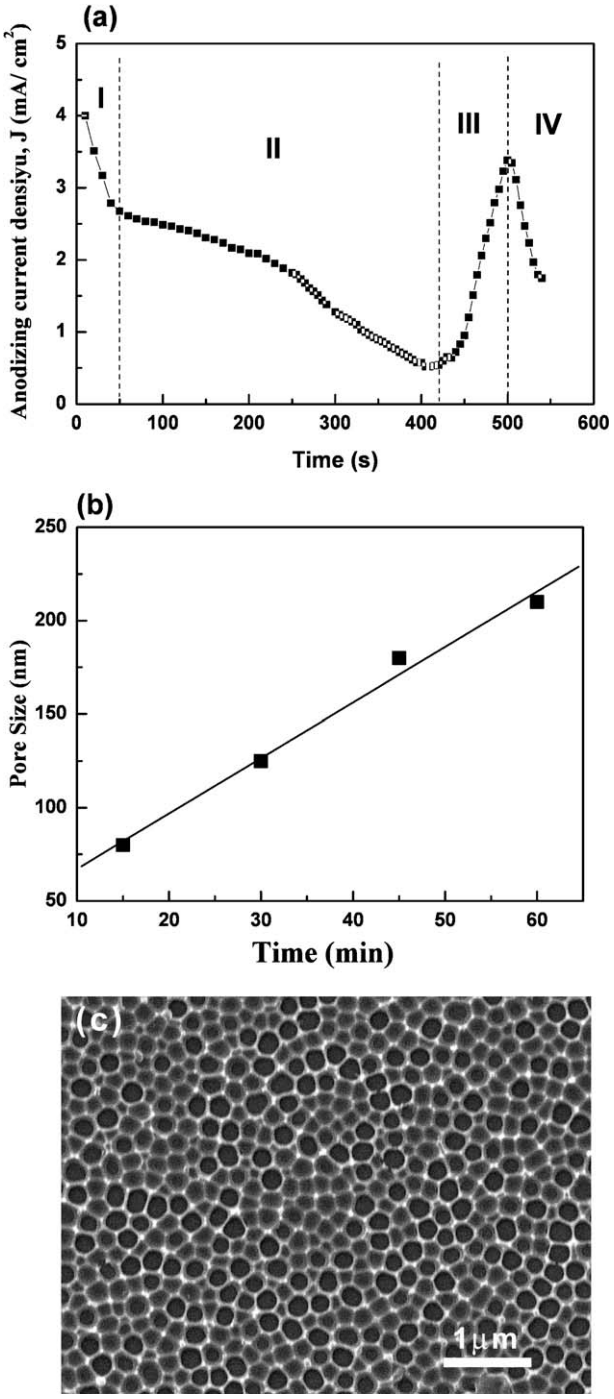

Fig. 1. (a) Current–time relationship during anodization process in phosphoric acid; (b) pore size–time relationship in pore widening-stage and (c) typical SEM micrograph for the resulted PAA layer on Si substrate.

After PAA process, using 5% phosphoric acid, which not only thins the alumina wall of PAA so as to enlarge pore size without changing pore-to-pore distance, but also etches the residual alumina layer formed at the bottom of pores, a pore-widening process was performed. In the pore-widening stage, the alumina in PAA was dissolved continuously such that the pore size increased linearly with anodizing time, shown as the plots in Fig. 1(b). The pore size of PAA increases from 65 to 230 nm as the anodizating time increases from 10 to 60 min, resulting in a PAA with the morphology shown in Fig. 1(c). A

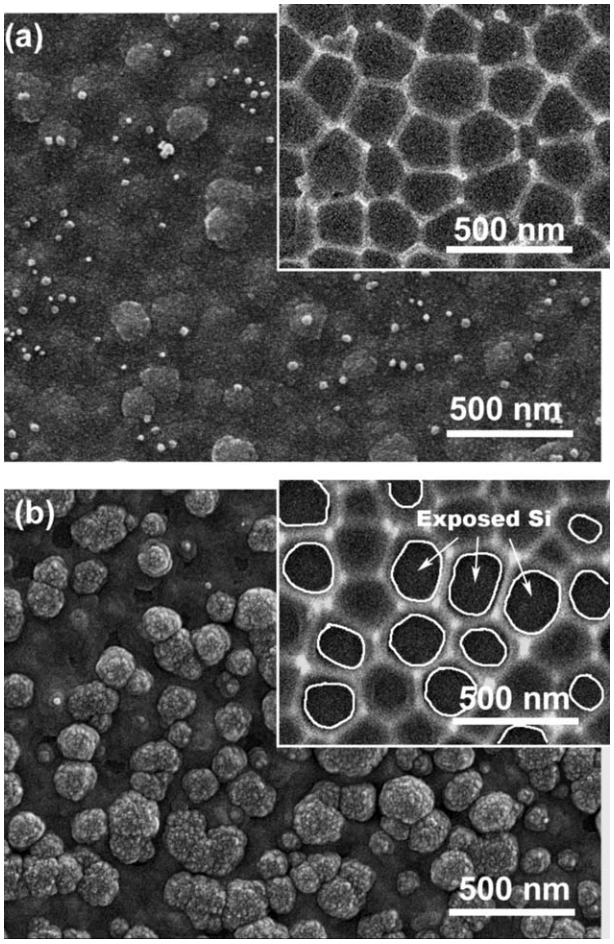

Fig. 2. SEM micrographs of nanodiamond seeding layer formed by bias-enhance-nucleation process for 10 min on PAA-coated Si substrate, where the PAA (a) contains a thin layer of alumina at the bottom pores; (b) contains no bottom alumina layer in the pore (the insets show the SEM micrograph of corresponding PAA templates used for growing nanodiamond seeding layer).

special throughing-process, i.e., etching in 10% phosphoric acid with reversed voltage is then applied to completely remove the bottom alumina layer without damaging the side wall of pores in PAA, so as to expose the Si-surface, which is crucial for the purpose of nucleating diamond on PAA substrate.

Fig. 2 demonstrates the importance of throughing-process in PAA fabrication process on the formation of diamond nuclei. SEM micrograph in Fig. 2(a) shows that, when the bottom of pores of PAA is still covered by a thin layer of alumina (inset, Fig. 2(a)), diamond seeds hardly grown when bias enhanced nucleation (BEN) process was performed for 10 min. In contrast, Fig. 2(b) indicates that nanodiamond aggregates about 100~200 nm in size were successfully formed on PAA containing silicon substrate by BEN process, when the bottom alumina layer in the pores of PAA was removed, exposing silicon surface (inset, Fig. 2(b)). It should be noted that the height of alumina cell is only about tens of nanometers, which is pronouncedly smaller than aggregates of nanodiamond about 200 nm in size. The grains of diamond are very small, about 20 nm in size.

The coverage of nanodiamond aggregates over the substrate and the size of aggregates increase with bias-enhanced-growth (BEG) process time, while the size of nanodiamond grains remains the same, which is shown in Fig. 3(a) for films grown on PAA pattern. Thus obtained nanodiamond films are labeled as NCD/PAA. The inset in Fig. 3(a) shows the SEM cross-sectional micrograph of 20 min-grown NCD/PAA films, clearly indicating that aggregates form hillocks with high aspect ratio. The Raman spectra of these nanodiamond films are typically shown in Fig. 4(a). It should be noted that the D-band at 1350 cm^{-1} and G-band at 1580 cm^{-1} are assigned as defective sp^3-bonded and sp^2-bonded carbon, respectively [15]. The broadening in these peaks is presumably induced by the strain effect due to nano-size nature of the nanodiamond grains. In contrast, the assignment of T_1*-, T_2*- and T_3*-bands are more controversial. It has been assigned as the nanodiamond grains [15] or the formation of trans-polyacetylene [16,17] layer in the surface of the grains. Nonetheless, the presents of these Raman peaks are closely related to the formation of nano-sized diamond grains.

To facilitate the comparison, the nanodiamond films were also grown on Si substrate directly without the formation of PAA, which are designated as non-patterned nanodiamond

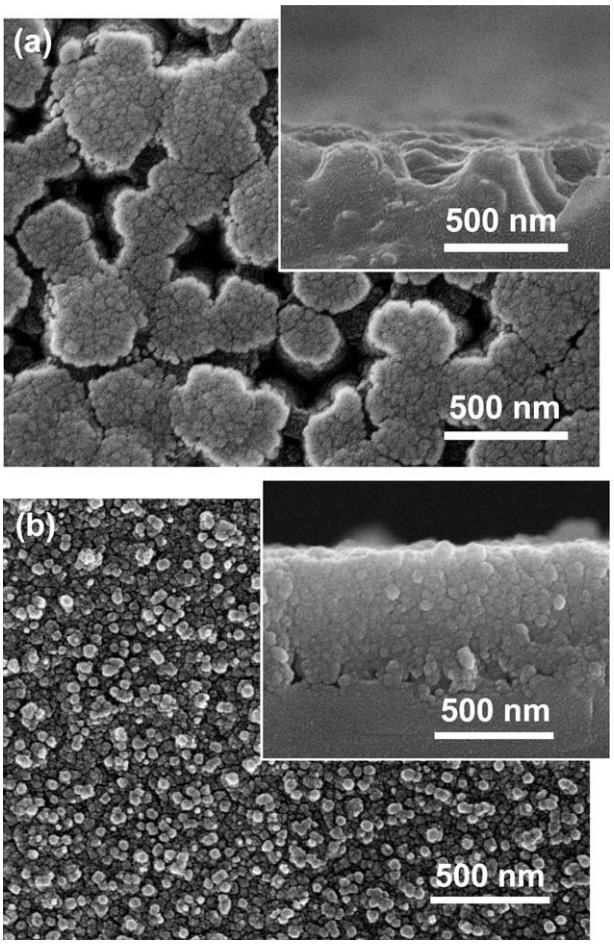

Fig. 3. SEM micrographs of nanodiamond films grown on (a) PAA patterned and (b) non-patterned Si substrate under −125 V bias for 20 min (the insets show the cross-section structure of corresponding nanodiamond films).

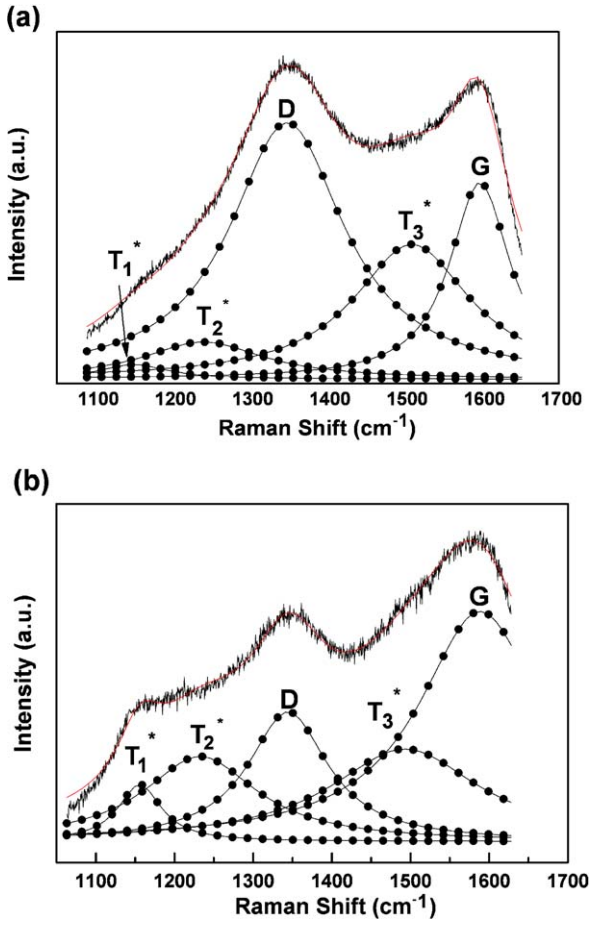

Fig. 4. Raman spectra and fittings for nanodiamond film grown on (a) PAA patterned and (b) non-patterned Si substrate under −125 V bias for 20 min.

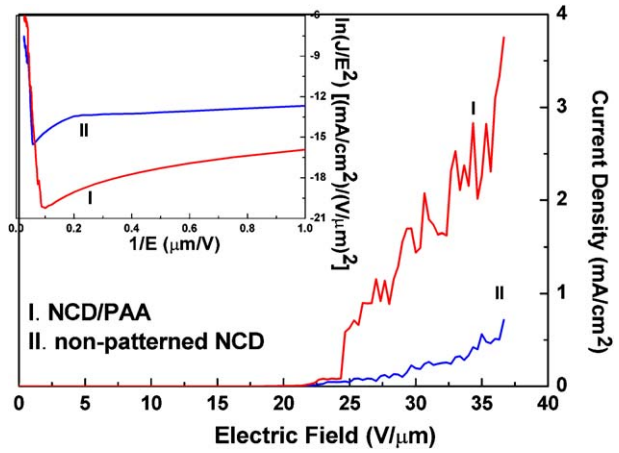

Fig. 5. Electron field emission properties of nanodiamond film grown on (I) PAA patterned and (II) non-patterned Si substrate.

films. Fig. 3(b) shows that such kind of nanodiamond films contain very uniform granular structure. The grain size, around 20∼30 nm, is slightly larger than that of the PAA-patterned nanodiamond films (Fig. 3(a)). Moreover, clusters of non-uniform size were formed for non-patterned nanodiamond films. In contrast, no clusters were formed within each aggregate in NCD/PAA films. Raman spectrum of the non-patterned nanodiamond film was shown in Fig. 4(b). Detail analysis on Raman spectra by fitting the curve with Lorentzian peaks at T_1*=1140 cm^{-1}, T_2*=1420 cm^{-1}, D=1350 cm^{-1}, T_3*=1480 cm^{-1} and G=1580 cm^{-1} [12,13] are listed in Table 1, illustrating the subtle change in relative content of the peaks. This table indicates that the non-patterned nanodiamond films contain marked larger proportion of trans-polyacetylene layer T_1*-, T_2*- and T_3*-bands. The significance of such a layer on the electron field emission properties of the nanodiamond films will be discussed shortly.

The PAA-patterned nanodiamond films (NCD/PAA) grown for a time interval shorter than 15 min possess essentially no electron field emission capacity (not shown), indicating that the NCD has not yet fully covered the Si substrates such that the NCD is not electrically connected to the Si substrate. However, the 20 min-grown nanodiamond films exhibit very good electron field emission properties, i.e, they can be turned on at $(E_0)_{PAA}$=10 V/μm, attaining $(J_e)_{PAA}$=3.8 mA/cm^2 at E_a=37 V/μm applied field (curve *I*; Fig. 5). In contrast, the non-patterned nanodiamond film possesses pronouncedly inferior electron field emission properties to the PAA-patterned one [$(E_0)_{Non}$=17 V/μm, $(J_e)_{Non}$=0.7 mA/cm^2 at E_a=37 V/μm]. It should be noted that the fluctuation in electrical field emission current density resulted from the small area of the anode, which is a 3 mm disk attached to a micrometer. However the results shown in Fig. 5 is consistently observed which illustrates clearly the benefit of PAA patterning process on improving electron field emission properties for nanodiamond films.

The important electron field emission parameters were exact from I–V curves shown in Fig. 5 and are listed in Table 2, which shows even more clearly that field enhancement factor (β) has been increased due to the utilization of PAA template and, therefore, pronouncedly decreases the turn-on field needed for triggering the electron field emission process. One of the factors for better electron field emission properties of PAA-patterned nanodiamond films is that the NCD/PAA contain hillocks which resulted from PAA patterns. The hillocks contain large proportion of sidewalls, which facilitate the transport of electrons from Si substrate to the top surface of

Table 1
Characteristics of the Raman spectra for the PAA-patterned and non-patterned nanodiamond films

Materials	T*$_1$-band (1150 cm^{-1}) (%)	T$_2$*-band (1240 cm^{-1}) (%)	D-band (1350 cm^{-1}) (%)	T*$_3$-band (1480 cm^{-1}) (%)	G-band (1580 cm^{-1}) (%)
PAA-patterned	1.6	7.2	46.9	25.3	19.0
Non-patterned	3.5	15.0	16.1	21.4	44.0

The Raman peaks were fitted using Larentz function [13], and the percentage of each peak band was calculated from the integral intensity of the peaks.

Table 2
Electron field emission properties of PAA-patterned and non-patterned nanodiamond films

Materials	E_0 (V/μm)	J_e (mA/cm^2)	Φ_e (eV)	β
PAA-patterned	10	3.8	0.0372	1.89
Non-patterned	17	0.7	0.0694	1

Electron field emission characteristics: E_0=turn-on field; J_e=emission current density; Φ_e= effective work function and β=field enhancement factor.

hillocks via surface conduction mechanism and, thereafter, improves markedly electron field emission capacity. Moreover, it is believed that the formation of larger proportion of trans-polyacetylene layer on the non-patterned nanodiamond films (Fig. 4(b)) is also a significant factor degrading the electron field emission properties of the materials. Restated, both the SEM microstructure and Raman structure have pronounced effect on the electron field emission properties of the nanodiamond films.

4. Conclusions

To enhance the electron field emission capacity of diamond films, porous anodic alumina (PAA) assisted growth process was used for patterning the nanocrystalline diamond (NCD), so as to increase the aspect ratio of the electron emission site and to improve the field enhancement factor. Porous anodic alumina (PAA) layer was first fabricated on Si substrate, The aluminum films were evaporated onto Si substrate and were anodized in 10% phosphoric acid. A two-step PAA process was adopted to improve the uniformity of the PAA layer. After the formation of PAA honeycomb pattern, the nanodiamond films were grown in a 2.45 GHz microwave plasma enhanced chemical vapor deposition (MPECVD) system, using CH_4/H_2 plasma. The morphologies of PAA and diamond films were characterized. The effect of the PAA layer on the electron field emission behavior of the nanodiamond films was discussed. The best electron field emission properties obtained is turn-on field E_0=10 V/μm, electron field emission current density J_e=3.8 mA/cm^2 at 37 V/μm applied field.

Acknowledgment

The authors would like to thank National Science Council, R.O.C. for the support of this research through the project No. NSC 93-2112-M-032-010.

References

[1] F. Benedic, M.B. Assouar, et al., Diamond Relat. Mater. 13 (2004) 347.
[2] Yen Chih Lee, Su Jien Lin, et al., J. Appl. Phys. 97 (2005) 054310.
[3] Y. Ando, Y. Nishibayashi, H. Furuta, et al., Diamond Relat. Mater. 12 (2003) 1681.
[4] Jerome P. Silverman, et al., J. Vac. Sci. Technol., B 15 (1997) 2117.
[5] M.A. McCord, et al., J. Vac. Sci. Technol., B 15 (1997) 2125.
[6] Y.F. Mei, G.G. Siu, et al., Phys. Lett., A 324 (2004) 479.
[7] Oded Rabin, Paul R. Herz, et al., Adv. Funct. Mater. 13 (8) (2003) 631.
[8] Mun Ja Kim, Tae Young Lee, et al., Diamond Relat. Mater. 12 (2003) 870.
[9] John C. Hulteen, David A. Treichel, et al., J. Phys. Chem., B 103 (1999) 3854.
[10] Mingliang Tian, Shengyong Xu, et al., Nano Lett. 5 (4) (2005) 697.
[11] A.P. Li, F. Muller, et al., J. Appl. Phys. 84 (11) (1998) 6023.
[12] R. Pfeiffer, H. Kuzmany, et al., Diamond Relat. Mater. 12 (2003) 268.
[13] N. Jiang, K. Eguchi, et al., J. Cryst. Growth 236 (2002) 577.
[14] A. Vander Ziel, Solid State Physical Electronics, Prentice-Hall, Englewood Cliffs, 1968, p. 144 P.
[15] E. Gonon, A. Gheeraert, F. Deneuvile, L. Fontaine, G. Abello, Luazeau, J. Appl. Phys. 8 (1995) 7509.
[16] A.C. Ferrari, J. Robertson, Phys. Rev., B 63 (2001) 121405.
[17] H. Kuzmany, R. Pfeiffer, N. Salk, B. Gunther, Carbon 42 (2004) 911.